IEICE TRANS. COMMUN., VOL.E100–B, NO.11 NOVEMBER 2017

PAPER

An Iterative Cancellation Technique for Adjacent Channel Interference Induced by Amplifier Nonlinearity in 60 GHz Band Wireless Communication Systems

Noboru OSAWA[†a)], ***Student Member***, **Shinsuke IBI**[†b)], ***Member***, ***and*** **Seiichi SAMPEI**[†c)], ***Fellow***

SUMMARY This paper proposes an iterative cancellation technique for adjacent channel interference (ACI), induced by amplifier nonlinearity in millimeter wave (mmW) communication systems. In mmW communications, a large spectrum leak is expected because of the amplifier nonlinearity, and such a spectrum leak disturbs multichannel utilization. In order to mitigate the ACI, iterative interference cancellation in the receiver side is designed in this paper. Typically, iterative interference cancellation is conducted by generating a soft replica of interference from the feedback of the decoder, and subtracting the replica from the received signals. In this case, the canceller must know the amplifier nonlinearity in order to regenerate a soft replica of ACI. In this paper, amplifier nonlinearity is estimated by subjecting the received pilot signals to polynomial regression. We reveal that using only pilot signals in estimating amplifier nonlinearity is insufficient for guaranteeing replica accuracy. To address this issue, the proposed scheme exploits the detected data sequence in the regression analysis. We demonstrate that the proposed ACI cancellation technique can effectively mitigate ACI in multichannel utilization.

key words: *millimeter wave, amplifier nonlinearity, adjacent channel interference, iterative canceller, nonlinearity estimation, multichannel access*

1. Introduction

The rapid growth of demand for high data rate wireless communication brings us to an extension of wireless resources in the spatial domain, as well as frequency domain [1]. Regarding this trend, researchers of wireless communication recognize the importance of three technologies; massive-dimensional signal processing in multiple-input multiple-output (MIMO) channels [2], millimeter-wave (mmW) transmissions as a new radio access technology (RAT) [3], and heterogeneous networks with the assistance of control/user (C/U) plane splitting [4]. Among them, the extension of frequency bandwidth in mmW is effective in meeting the rapid increase of mobile traffic and peak user rate.

The mmW transmission has been in development for a long time. In 2005, an implementation of mmW into CMOS triggered the current boom of higher-frequency utilization [5]–[7]. Unlike scarce microwave bands, the mobile stations (STAs) are capable of occupying extremely wide bandwidths in mmW bands. For example, in IEEE 802.11ad, four channels with 2.16 GHz bandwidths at 60 GHz are available [8]. Owing to the very wide bandwidths, the channel capacity is significantly improved, even without sophisticated signal processing. Furthermore, IEEE 802.11ay is being developed as a new standard for 60 GHz band communication systems.

However, mmW transmission has serious disadvantages; such as a huge path-loss, especially in 60 GHz bands. Thus, mmW systems require power-efficient amplifiers to alleviate the penalty of the path-loss. A straightforward method to improve the power efficiency is to reduce the output back-off (OBO) of the amplifier as much as possible [9]. However, if the peak to average power ratio (PAPR) of the input signal is relatively high, a small OBO induces nonlinear distortion, resulting in a huge spectrum leak to out-of-bands. Considering the balance between good power efficiency and suppression of out-of-band radiation, as well as the cost of the power amplifier, the spectral mask of IEEE 802.11ad is relaxed, when compared with conventional wireless local area network (LAN) standards.

Several digital predistortion techniques in the transmitter side have been proposed to alleviate the nonlinear distortion [10]–[12]. However, IEEE 802.11ad has been already commercialized and some terminals without predistortion is widely spread. Therefore, the link connections are suffering from ACI in some geographical communication topologies. A straightforward approach to avoid ACI is to prohibit utilizations of adjacent channels in four available channels. As the result, the sum-rate of multiple users becomes half. Our proposed ACI canceller is capable of addressing the penalty. We can expect that the IEEE 802.11ad users will increase near future. In this case, ACI canceller in the receiver side might play a vital role to improve the sum-rate capacity.

Iterative interference cancellation with the assistance of channel decoder feedback is a typical approach to suppress the interference observed in the uplink access point (AP) [13], [14]. With this method, soft interference replicas are generated from the decoder feedback, which is then subtracted from the received signal. Thus, this paper proposes an iterative cancellation scheme for the ACI, with the assistance of a nonlinearity estimator. The ACI included in the transmitted signals can be described as a wide band signal model. Thus, one of the contributions of this paper is detailed description of the oversampled signal and system models.

Manuscript received August 17, 2016.
Manuscript revised February 11, 2017.
Manuscript publicized May 15, 2017.

[†]The authors are with the Graduate School of Engineering, Osaka University, Suita-shi, 565-0871 Japan.
a) E-mail: osawa@wcs.comm.eng.osaka-u.ac.jp
b) E-mail: ibi@comm.eng.osaka-u.ac.jp
c) E-mail: sampei@comm.eng.osaka-u.ac.jp

DOI: 10.1587/transcom.2016EBT0006

Furthermore, because interference signals experience not only the nonlinear distortion at the transmit amplifier, but also frequency selective fading, the ACI replica generator must accurately estimate characteristics of both amplifier nonlinearity and frequency selective fading behavior. In order to estimate amplifier nonlinearity, the proposed scheme employs polynomial regression analysis. According to the analysis, we came across an essential fact; namely, that polynomial regression using only a pilot sequence is insufficient for ACI cancellation. This is because the pilot sequence has a smaller PAPR than the data sequence. Therefore, in this paper, a nonlinearity estimation mechanism that uses the data sequence in the regression analysis is designed.

The rest of this paper is organized as follows. In Sect. 2, we describe the system model of mmW transmission on a single channel. Then, the single channel receiver is extended to the iterative multichannel receiver with ACI canceller, and estimation method of power amplifier nonlinearity is described in Sect. 3. In Sect. 4, firstly, the behavior of the proposed scheme is characterized in terms of the bit error rate (BER) using link level computer simulations. Thereafter, system level computer simulations are conducted to confirm that the proposed scheme can improve the throughput performance. Finally, the conclusions are presented in Sect. 5.

2. Signal Model on Single Channel

2.1 Transmitted Signal Model

Figure 1 shows a schematic of a typical single carrier (SC) transmitter. At the transmitter, information bit block $\boldsymbol{b}$ is encoded by the low density parity check (LDPC) codes [15], [16], to generate a coded bit stream $\boldsymbol{c}$. Then, $\boldsymbol{c}$ is mapped to a data symbol block that is denoted by $\boldsymbol{s}_\mathrm{d} = [s_\mathrm{d}(0), \ldots, s_\mathrm{d}(k), \ldots, s_\mathrm{d}(K_\mathrm{d}-1)]^\mathrm{T}$. The block length is K_d symbols and the average symbol energy $\mathbb{E}\{|s_\mathrm{d}(k)|^2\}$ is denoted by E_s. Note that $\cdot^\mathrm{T}$ represents the transpose of a vector or matrix and $\mathbb{E}\{\cdot\}$ denotes the expectation. Obeying the IEEE 802.11ad signal format [8], 64 samples of the Golay code [17] $\boldsymbol{g}_\mathrm{d}$ are appended to the head of each data symbol block, having $K_\mathrm{d} = 448$ as a guard interval (GI).

Before transmitting this block with a length of 512 samples, an SC preamble consisting of the short training field (STF) and channel estimation field (CE), is transmitted. We assume here that the time and frequency synchronizations are perfect, and here we deal only with the CE part in SC preamble. The CE is constructed from three types of Golay code as $\boldsymbol{s}_\mathrm{p} = [\boldsymbol{g}_{\mathrm{p}0}^\mathrm{T}, \boldsymbol{g}_{\mathrm{p}1}^\mathrm{T}, \boldsymbol{g}_{\mathrm{p}2}^\mathrm{T}]^\mathrm{T}$, where $\boldsymbol{g}_{\mathrm{p}0}$ and $\boldsymbol{g}_{\mathrm{p}1}$ are 512 samples of column vectors, and $\boldsymbol{g}_{\mathrm{p}2}$ is 128 samples of a column vector. In addition, $\boldsymbol{g}_{\mathrm{p}2}$ is identical to the first 128 samples of the $\boldsymbol{g}_{\mathrm{p}0}$ and $\boldsymbol{g}_{\mathrm{p}1}$, so that it plays a role of cyclic prefix (CP). For ease of notations, we define a common transmitted block $\boldsymbol{s} = [s(0), \ldots, s(k), \ldots, s(K-1)]^\mathrm{T}$, which is expressed as

$$\boldsymbol{s} = \begin{cases} \left[\boldsymbol{s}_\mathrm{d}^\mathrm{T}, \quad \boldsymbol{g}_\mathrm{d}^\mathrm{T}\right]^\mathrm{T}, & \text{(data sequence)} \\ \boldsymbol{s}_\mathrm{p}^-, & \text{(pilot sequence),} \end{cases} \tag{1}$$

where $\boldsymbol{s}_\mathrm{p}^-$ denotes a partial block of $\boldsymbol{s}_\mathrm{p}$, which removes the first 128 samples from $\boldsymbol{s}_\mathrm{p}$. Note that we have $K = 512$ when $\boldsymbol{s}$ represents the data sequence, and $K = 1024$ when $\boldsymbol{s}$ represents the pilot sequence. Owing to the CP samples placed in front of $\boldsymbol{s}$, linear convolutional operations applied to $\boldsymbol{s}$ can be expressed as circular convolutions.

In order to apply the pulse shaping filter to the transmitted block, $\boldsymbol{s}$ is up-sampled. In the mmW systems, the up-sampling rate is usually limited to two-fold. This is because of the difficulty of hardware implementations for broadband signals. The operation of U-fold up-sampling inserts U-1 zero elements between samples. Thus, the two-fold up-sampled block is expressed as

$$[s(0), 0, s(1), 0, \ldots, 0, s(K-1), 0]^\mathrm{T} = \boldsymbol{O}_2\boldsymbol{s}, \tag{2}$$

where $\boldsymbol{O}_2$ is a $2K \times K$ matrix for twofold up-sampling. A transmit pulse shaping filter is then applied to $\boldsymbol{O}_2\boldsymbol{s}$, which is denoted as

$$\boldsymbol{x} = \boldsymbol{C}_\mathrm{TX}\boldsymbol{O}_2\boldsymbol{s}, \tag{3}$$

where $\boldsymbol{C}_\mathrm{TX}$ is a circulant filter matrix for pulse shaping. Thereafter, the digital signal block $\boldsymbol{x}$ is converted to an analog signal by the digital-to-analog converter (DAC). In this paper, we approximately express the DAC output as $\boldsymbol{O}_U\boldsymbol{x}$, where $\boldsymbol{O}_U$ is a $2KU \times 2K$ up-sampling matrix. After applying the low pass filter (LPF) to $\boldsymbol{O}_U\boldsymbol{x}$, we have

$$\boldsymbol{v} = \boldsymbol{\Gamma}_\mathrm{TX}\boldsymbol{O}_U\boldsymbol{x}, \tag{4}$$

where $\boldsymbol{\Gamma}_\mathrm{TX}$ is a $2UK \times 2UK$ circulant LPF matrix of the transmitter. The resultant analog signal $\boldsymbol{v} = [v(0), \ldots, v(m), \ldots, v(M-1)]^\mathrm{T}$, where $M = 2UK$, is then converted to the radio frequency (RF) signal by the local oscillator, and is thereafter input to a power amplifier.

Let the nonlinear function expressed by the equivalent low pass system be $G[\cdot]$; the output of the nonlinear amplifier can then be expressed as

$$\tilde{v}(m) = G[v(m)]. \tag{5}$$

After the RF signal is band-limited by a band pass filter (BPF), it is sent to the receiver via frequency selective fading channels.

2.2 Received Signal Model

A single channel receiver without an ACI canceller is depicted in Fig. 2. At first, the received signal is filtered by a BPF and the received signal level is controlled by an automatic gain control (AGC). The received signal block expressed as an equivalent low-pass system is given by

$$\boldsymbol{z} = \boldsymbol{\Psi}\tilde{\boldsymbol{v}} + \boldsymbol{\omega}, \tag{6}$$

where $\boldsymbol{\omega} = [\omega(1), \ldots, \omega(m), \ldots, \omega(M)]^\mathrm{T}$ is a complex-valued additive white Gaussian noise (AWGN) vector, whose elements obey the zero mean and variance of the one-sided noise power spectrum density N_0. Furthermore, $\boldsymbol{\Psi}$ is an

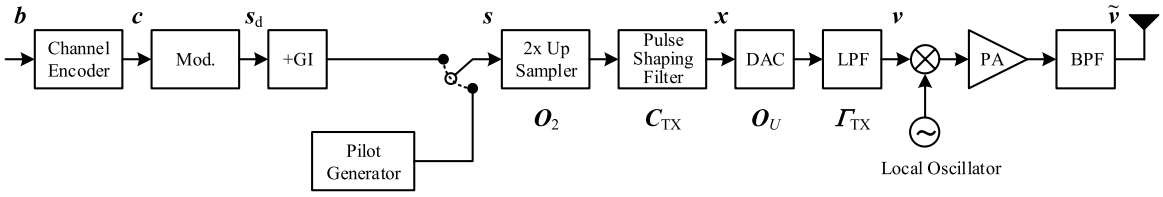

Fig. 1 Schematic of single carrier transmitter.

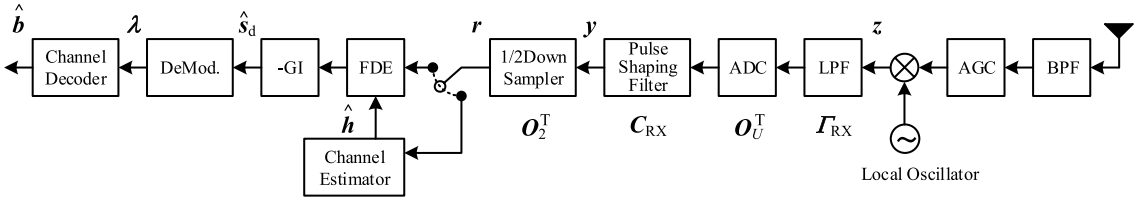

Fig. 2 Schematic of single carrier receiver.

$M \times M$ circulant channel matrix for frequency selective fading channels.

The received signal $\boldsymbol{z}$ is filtered by an $M \times M$ LPF matrix $\boldsymbol{\Gamma}_{\mathrm{RX}}$, then an analog-to-digital converter (ADC) captures the digital samples with two-fold of the symbol rate, which is obtained by $O_U^{\mathrm{T}}\boldsymbol{\Gamma}_{\mathrm{RX}}\boldsymbol{z}$. Note that the operation of down-sampling is denoted by $\boldsymbol{O}_U^{\mathrm{T}}$, which is an inverse matrix of the up-sampling matrix, because of $\boldsymbol{O}_U^{\mathrm{T}}\boldsymbol{O}_U = \boldsymbol{I}$. After the ADC operation, the pulse shaping filter, which is denoted by the circulant matrix $\boldsymbol{C}_{\mathrm{RX}}$, is applied to the sampled block. The resultant shaped block $\boldsymbol{y}$ is given by

$$\boldsymbol{y} = \boldsymbol{C}_{\mathrm{RX}}\boldsymbol{O}_U^{\mathrm{T}}\boldsymbol{\Gamma}_{\mathrm{RX}}z. \tag{7}$$

Then, $\boldsymbol{y}$ is down-sampled to the symbol rate, which is expressed as

$$\boldsymbol{r} = \boldsymbol{O}_2^{\mathrm{T}}\boldsymbol{y}, \tag{8}$$

By denoting an error vector $\boldsymbol{\delta} = \tilde{\boldsymbol{v}} - \boldsymbol{v}$ caused by the nonlinear distortion at the power amplifier, (8) is rewritten as

$$\boldsymbol{r} = \boldsymbol{H}\boldsymbol{s} + \boldsymbol{\kappa} + \boldsymbol{n}, \tag{9}$$

where $\boldsymbol{H}$ is a channel matrix in the symbol rate domain, $\boldsymbol{\kappa}$ is a nonlinear distortion component vector, and $\boldsymbol{n}$ is a noise component vector, which are respectively given by

$$\boldsymbol{H} = \boldsymbol{O}_2^{\mathrm{T}}\boldsymbol{C}_{\mathrm{RX}}\boldsymbol{O}_U^{\mathrm{T}}\boldsymbol{\Gamma}_{\mathrm{RX}}\boldsymbol{\Psi}\boldsymbol{\Gamma}_{\mathrm{TX}}\boldsymbol{O}_U\boldsymbol{C}_{\mathrm{TX}}\boldsymbol{O}_2, \tag{10}$$

$$\boldsymbol{\kappa} = \boldsymbol{O}_2^{\mathrm{T}}\boldsymbol{C}_{\mathrm{RX}}\boldsymbol{O}_U^{\mathrm{T}}\boldsymbol{\Gamma}_{\mathrm{RX}}\boldsymbol{\Psi}\boldsymbol{\delta}, \tag{11}$$

$$\boldsymbol{n} = \boldsymbol{O}_2^{\mathrm{T}}\boldsymbol{C}_{\mathrm{RX}}\boldsymbol{O}_U^{\mathrm{T}}\boldsymbol{\Gamma}_{\mathrm{RX}}\boldsymbol{\omega}. \tag{12}$$

Channel estimation and signal detection are performed using $\boldsymbol{r}$ in (9).

2.3 Channel Estimation

The received symbol block $\boldsymbol{r}$ of a pilot block $\boldsymbol{s}_{\mathrm{p}}$ is delivered to the channel estimator for capturing a channel impulse response (CIR). Let us the denote CIR vector as $\boldsymbol{h} = [h(0), \ldots, h(l), \ldots, h(L-1), 0, \ldots, 0]^{\mathrm{T}}$, which is the first column vector of the circulant channel matrix $\boldsymbol{H}$. Note that L is the channel memory of frequency selective fading. We assume here that the CIR memory length L is not larger than the GI length L_{GI} ($L < L_{\mathrm{GI}}$). The CIR vector with a length of $L_{\mathrm{GI}} + 1$ is then estimated using circulant matrix $\boldsymbol{S}$, which is a $K \times (L_{\mathrm{GI}} + 1)$ matrix, expressed as

$$\boldsymbol{S} = \begin{bmatrix} s_{\mathrm{p}}^{-}(0) & s_{\mathrm{p}}^{-}(K-1) & s_{\mathrm{p}}^{-}(K-2) & \cdots & s_{\mathrm{p}}^{-}(K-L_{\mathrm{GI}}) \\ s_{\mathrm{p}}^{-}(1) & s_{\mathrm{p}}^{-}(0) & s_{\mathrm{p}}^{-}(K-1) & \cdots & s_{\mathrm{p}}^{-}(K-L_{\mathrm{GI}}+1) \\ \vdots & \vdots & \vdots & \ddots & \vdots \\ s_{\mathrm{p}}^{-}(K-1) & s_{\mathrm{p}}^{-}(K-2) & s_{\mathrm{p}}^{-}(K-3) & \cdots & s_{\mathrm{p}}^{-}(K-L_{\mathrm{GI}}-1) \end{bmatrix}. \tag{13}$$

The estimated CIR vector $\hat{\boldsymbol{h}}$ is calculated by multiplying the pseudo-inverse of $\boldsymbol{S}$ by the received pilot block $\boldsymbol{r}$. Owing to the significant sharpness of the autocorrelation of the Golay sequence [17], the pseudo-inverse of $\boldsymbol{S}$ is simply given by $\boldsymbol{S}^{\mathrm{H}}/K$. Note that $\cdot^{\mathrm{H}}$ denotes a conjugate transpose of the matrix. As a result, $\hat{\boldsymbol{h}}$ is obtained by

$$\hat{\boldsymbol{h}} = \left[\frac{1}{K}\left(\boldsymbol{S}^{\mathrm{H}}\boldsymbol{r}\right)^{\mathrm{T}}, 0, \ldots, 0\right]^{\mathrm{T}}, \tag{14}$$

where $K - L_{\mathrm{GI}} - 1$ zeros are appended to meet the discrete Fourier transform (DFT) window size.

2.4 Signal Detection

The received symbol block $\boldsymbol{r}$ of a data block $\boldsymbol{s}_{\mathrm{d}}$, is equalized by the simple frequency domain equalizer (FDE). At first, DFT is applied to the received symbol block $\boldsymbol{r}$. Then, the DFT output is multiplied by a weight matrix $\boldsymbol{W}$ for FDE, and retransformed into the time domain using the inverse discrete Fourier transform (IDFT) operation. As a result, we have

$$\left[\ \hat{\boldsymbol{s}}_{\mathrm{d}}^{\mathrm{T}},\quad \hat{\boldsymbol{g}}_{\mathrm{d}}^{\mathrm{T}}\ \right]^{\mathrm{T}} = \boldsymbol{F}^{\mathrm{H}}\boldsymbol{W}\boldsymbol{F}\boldsymbol{r}, \tag{15}$$

where $\boldsymbol{F}$ denotes the DFT matrix. The weight matrix $\boldsymbol{W}$ is a

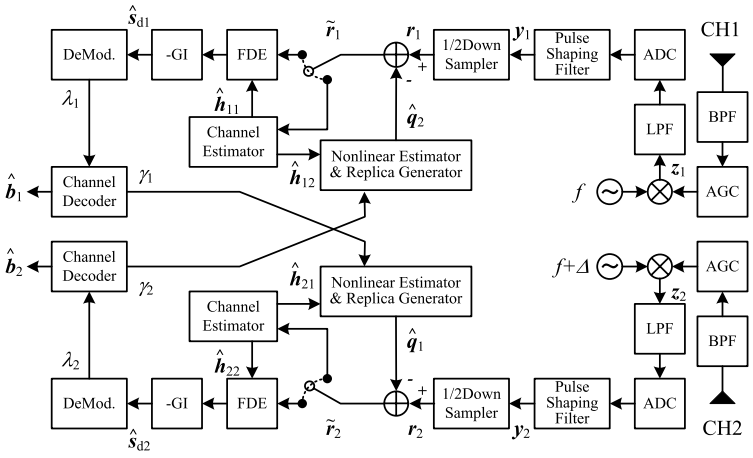

Fig. 3 A schematic of the multichannel receiver with the ACI canceller.

diagonal matrix derived from the estimated CIR $\hat{\boldsymbol{h}}$. According to the minimum mean square error (MMSE) criterion, the k-th diagonal element of $\boldsymbol{W}$ is given by

$$w(k) = \frac{\hat{\xi}^*(k)}{\left|\hat{\xi}(k)\right|^2 + (N_0 + I)/E_\mathrm{s}}, \tag{16}$$

where $\cdot^*$ denotes the conjugate of the element. Moreover, I is the interference power in a case where ACI exists, and it has to be measured in advance. Furthermore, $\hat{\xi}(k)$ is the k-th element of vector $\hat{\boldsymbol{\xi}}$, where $\hat{\boldsymbol{\xi}}$ is given by

$$\hat{\boldsymbol{\xi}} = \sqrt{K}\boldsymbol{F}\hat{\boldsymbol{h}}. \tag{17}$$

After removing the GI $\hat{\boldsymbol{g}}_\mathrm{d}$ from the FDE output, $\hat{\boldsymbol{s}}_\mathrm{d}$ is extracted. At the demodulator, the log likelihood ratio (LLR) block $\boldsymbol{\lambda}$ is computed from $\hat{\boldsymbol{s}}_\mathrm{d}$. After yielding the LLRs to the channel decoder, information bits are detected with the aid of forward error correction.

3. Iterative Multichannel Receiver

3.1 Received Signal Model

Figure 3 illustrates a configuration of the proposed multichannel iterative receiver with a function of ACI cancellation. Let us consider a situation wherein two stations, STA1 and STA2, simultaneously transmit their own signals to a common AP, over adjacent channels. Furthermore, STA1 occupies CH1 with a center frequency of f, and STA2 occupies CH2 with a center frequency of $f + \Delta$. In IEEE 802.11ad, the channel spacing Δ is 2.16 GHz. For ease of analysis, we assume that the receiving timings of STA1 and STA2 are perfectly synchronized. For ease of notations, each variable with the subscription $i \in \{1, 2\}$ represents a variable for STAi in cases of transmission, or a variable for CHi in cases of reception.

The received signal on CH1 is expressed as

$$\boldsymbol{r}_1 = \boldsymbol{H}_{11}\boldsymbol{s}_1 + \boldsymbol{\kappa}_1 + \boldsymbol{n}_1 + \boldsymbol{q}_2, \tag{18}$$

where $\boldsymbol{H}_{11}$ represents a channel matrix with respect to a propagation path between STA1 and AP, over CH1. Furthermore, $\boldsymbol{q}_2$ denotes an ACI component coming from STA2, which is given by

$$\boldsymbol{q}_2 = \boldsymbol{O}_2^\mathrm{T}\boldsymbol{C}_\mathrm{RX}\boldsymbol{O}_U^\mathrm{T}\boldsymbol{\Gamma}_\mathrm{RX}\boldsymbol{\Phi}_{12}\boldsymbol{\Psi}_{12}\tilde{\boldsymbol{v}}_2, \tag{19}$$

where $\boldsymbol{\Psi}_{12}$ denotes a channel matrix with respect to a propagation path between STA2 and AP, over CH1. Moreover, $\boldsymbol{\Phi}_{12}$denotes a diagonal matrix of phase rotations, caused by a frequency offset between CH1 and CH2, whose m-th diagonal element is $\exp[j2\pi\Delta Tm/(2U)]$, where j denotes the imaginary unit $\sqrt{-1}$ and T denotes the symbol interval. In an analogous way, received ACI in $\boldsymbol{r}_2$ is expressed as

$$\boldsymbol{q}_1 = \boldsymbol{O}_2^\mathrm{T}\boldsymbol{C}_\mathrm{RX}\boldsymbol{O}_U^\mathrm{T}\boldsymbol{\Gamma}_\mathrm{RX}\boldsymbol{\Phi}_{21}\boldsymbol{\Psi}_{21}\tilde{\boldsymbol{v}}_1. \tag{20}$$

The received signal $\boldsymbol{r}_i$ is equalized, demodulated, and decoded. At this stage, a soft replica of ACI is created by the extrinsic LLR that was obtained by the received signals on the other channel. Based on the reliability of $\boldsymbol{\gamma}_i$, the soft replica of the ACI component (19) is computed as $\hat{\boldsymbol{q}}_i$ at the soft replica generator. The derived soft value $\hat{\boldsymbol{q}}_i$ is then subtracted from $\boldsymbol{r}_{i'}$ (when $i = 1$, $i' = 2$ and when $i = 2$, $i' = 1$), resulting in $\tilde{\boldsymbol{r}}_{i'} = \boldsymbol{r}_{i'} - \hat{\boldsymbol{q}}_i$. Based on the turbo principle [18], the iterative detection between the decoder and the ACI canceller is capable of improving the accuracy of ACI cancellation. Note that $\tilde{\boldsymbol{r}}_{i'} = \boldsymbol{r}_{i'}$ at the first iteration process, because no *a-priori* information is provided by the channel decoder.

Let us consider the case when the time synchronization is imperfect. In IEEE 802.11ad, the MAC layer protocols are synchronized by beacon signals. In the system model, multiple channels are utilized in one AP. Therefore, the single AP can simultaneously send beacon signals over all channels. This structure enables to synchronize coarsely. The ACI canceller is valid if total time of timing error caused by the coarse synchronization and maximum delay of channel impulse response is within the length of CP. We assume that the total error time is within the CP length.

The generation of $\hat{\boldsymbol{q}}_i$ at the soft replica generator plays a

vital role in the iterative receiver. Equation (19) implies that a perfect replica $\hat{\boldsymbol{q}}_2 = \boldsymbol{q}_2$ is obtained if knowledge of $\boldsymbol{\Psi}_{12}$ and $\tilde{\boldsymbol{v}}_2 = G[\boldsymbol{v}_2]$ is completely captured. Therefore, we focus on the detailed methodology to cancel the ACI, in terms of estimations of channel state $\boldsymbol{\Psi}_{ii'}$ and the nonlinearity function $G[\cdot]$.

3.2 Estimation of Nonlinearity in the Power Amplifier

At the power amplifier, both the amplitude and phase of the input signal experience nonlinear distortions; the nonlinearity is often characterized by an amplitude modulation to amplitude modulation (AM-AM) model, and an amplitude modulation to phase modulation (AM-PM) model, respectively. In this paper, we utilize the modified Rapp model, which is approved by the IEEE 802.11ad task group [19]. Here, we rewrite $v_i(m)$ in (4) as

$$v_i(m) = |v_i(m)| \exp\left[j\theta_i(m)\right], \tag{21}$$

where $\theta_i(m)$ denotes the phase of $v_i(m)$. As a result, (5) is rewritten as

$$G\left[v_i(m)\right] = G_{\mathrm{AM}}\left[v_i(m)\right] \exp\left[j\left(\theta_i(m) + G_{\mathrm{PM}}\left[v_i(m)\right]\right)\right], \tag{22}$$

where $G_{\mathrm{AM}}[v_i(m)]$ and $G_{\mathrm{PM}}[v_i(m)]$ denote AM-AM and AM-PM functions, which are respectively given by

$$G_{\mathrm{AM}}\left[v_i(m)\right] = \frac{\alpha_1 \left|v_i(m)\right|}{\left[1 + \left(\alpha_1 \left|v_i(m)\right| / \alpha_2\right)^{2\alpha_3}\right]^{\frac{\alpha_3}{2}}}, \tag{23}$$

$$G_{\mathrm{PM}}\left[v_i(m)\right] = \frac{\beta_1 \left|v_i(m)\right|^{\beta_2}}{\left[1 + \left(\left|v_i(m)\right| / \beta_3\right)^{\beta_4}\right]}. \tag{24}$$

The parameters of the above equations are set as $\alpha_1 = 1.9$, $\alpha_2 = 1.4$, $\alpha_3 = 1.81$, and $\beta_1 = -4.8$, $\beta_2 = 3.8$, $\beta_3 = 1.5$, $\beta_4 = 3.7$, in this paper [19]. In this configuration, the OBO becomes 0.6 dB when the averaged energy of symbols E_{s} is 1.0, and the leakage power increases to near the limit of the spectral mask.

To estimate the nonlinearity included in the received signal $\tilde{v}_i(m)$, a polynomial approximation [20] is applied to $\tilde{v}_i(m)$, which is given by

$$\begin{aligned}\tilde{v}_i(m) &= G\left[v_i(m)\right] \approx \bar{G}_i\left[v_i(m)\right] \\ &= a_1 v_i(m) + a_2 v_i(m)\left|v_i(m)\right|^2 + a_3 v_i(m)\left|v_i(m)\right|^4,\end{aligned} \tag{25}$$

where a_1, a_2, and a_3 are polynomial coefficients. In a vector form of (25), we have

$$\tilde{\boldsymbol{v}}_i = \bar{G}_i\left[\boldsymbol{v}_i\right] = a_1 \boldsymbol{v}_i + a_2 \boldsymbol{v}_i^{(3)} + a_3 \boldsymbol{v}_i^{(5)}, \tag{26}$$

where $\boldsymbol{v}_i^{(3)}$ and $\boldsymbol{v}_i^{(5)}$ denote the third and fifth order vectors, which are given by

$$\begin{aligned}\tilde{\boldsymbol{v}}_i^{(3)} &= [v_i(0)|v_i(0)|^2, \ldots, v_i(m)|v_i(m)|^2 \\ &\quad , \ldots, v_i(M-1)|v_i(M-1)|^2],\end{aligned} \tag{27}$$

$$\begin{aligned}\tilde{\boldsymbol{v}}_i^{(5)} &= [v_i(0)|v_i(0)|^4, \ldots, v_i(m)|v_i(m)|^4 \\ &\quad , \ldots, v_i(M-1)|v_i(M-1)|^4].\end{aligned} \tag{28}$$

On the basis of (26), a_1, a_2, and a_3 are estimated using regression analysis, for the sake of capturing the amplifier nonlinearity behavior. According to regression analysis based on the MMSE criteria, the optimal parameters a_1, a_2, and a_3 are obtained by minimizing the cost function $|\boldsymbol{z}_i - \boldsymbol{\Psi}_{ii}\bar{G}_i[v_i]|^2$.

However, it is infeasible to estimate the analog domain channel matrix $\boldsymbol{\Psi}_{ii}$, because the up-sampling rate is insufficient for wide band channel estimation. To address the infeasibility, we focus on the received block $\boldsymbol{y}_i$, not $\boldsymbol{z}_i$. In this case, (7) is approximated as

$$\boldsymbol{y}_i \approx \bar{\boldsymbol{H}}_{ii}\boldsymbol{x}_i + \bar{\boldsymbol{\kappa}}_i + \bar{\boldsymbol{n}}_i, \tag{29}$$

where $\bar{\boldsymbol{H}}_{ii}$, $\bar{\boldsymbol{\kappa}}_i$, and $\bar{\boldsymbol{n}}_i$ are respectively given by

$$\bar{\boldsymbol{H}}_{ii} = \boldsymbol{C}_{\mathrm{RX}}\boldsymbol{O}_U^{\mathrm{T}}\boldsymbol{\Gamma}_{\mathrm{RX}}\boldsymbol{\Psi}_{ii}\boldsymbol{\Gamma}_{\mathrm{TX}}\boldsymbol{O}_U\boldsymbol{C}_{\mathrm{TX}}, \tag{30}$$

$$\bar{\boldsymbol{\kappa}}_i = \boldsymbol{C}_{\mathrm{RX}}\boldsymbol{O}_U^{\mathrm{T}}\boldsymbol{\Gamma}_{\mathrm{RX}}\boldsymbol{\Psi}_{ij}\boldsymbol{\delta}_j, \tag{31}$$

$$\bar{\boldsymbol{n}}_i = \boldsymbol{C}_{\mathrm{RX}}\boldsymbol{O}_U^{\mathrm{T}}\boldsymbol{\Gamma}_{\mathrm{RX}}\boldsymbol{\omega}_i. \tag{32}$$

Let us rewrite (29) as

$$\boldsymbol{y}_i = \bar{\boldsymbol{H}}_{ii}\tilde{\boldsymbol{x}}_i + \bar{\boldsymbol{n}}_i, \tag{33}$$

where $\tilde{\boldsymbol{x}}_i$ denotes the symbol block that is affected by nonlinear distortions, and is expressed as $\tilde{\boldsymbol{x}}_i = \boldsymbol{x}_i + \left(\bar{\boldsymbol{H}}_{ii}\right)^{-1}\bar{\boldsymbol{\kappa}}_i$.

We then approximate $\tilde{\boldsymbol{x}}_i$ in the same way as (26), and we obtain

$$\tilde{\boldsymbol{x}}_i \approx \bar{G}_i\left[\boldsymbol{x}_i\right] = a_1\boldsymbol{x}_i + a_2\boldsymbol{x}_i^{(3)} + a_3\boldsymbol{x}_i^{(5)}. \tag{34}$$

where $\boldsymbol{x}_i^{(3)}$ and $\boldsymbol{x}_i^{(5)}$ are the third and fifth order vectors, which are defined in the same way as $\boldsymbol{v}_i^{(3)}$ and $\boldsymbol{v}_i^{(5)}$. In this case, the cost function for regression is given by $\left|\boldsymbol{y}_i - \bar{\boldsymbol{H}}_{ii}\bar{G}_i\left[\boldsymbol{x}_i\right]\right|^2$. However, it is still difficult to perfectly capture the up-sampling domain channel matrix $\bar{\boldsymbol{H}}_{ii}$. According to Sect. 2.3, we have only estimated CIR $\hat{\boldsymbol{h}}_{ii}$ at the symbol rate T. Approximating $\bar{\boldsymbol{H}}_{ii}$ by $\boldsymbol{O}_2\hat{\boldsymbol{h}}_{ii}$, we have an alternative circulant matrix $\hat{\bar{\boldsymbol{H}}}_{ii}$, whose first column vector is $\boldsymbol{O}_2\hat{\boldsymbol{h}}_{ii}$. Eventually, the minimization problem for the nonlinearity estimation of the power amplifier is expressed as

$$\min_{a_1,a_2,a_3}\left|\boldsymbol{y}_i - \left[a_1\hat{\bar{\boldsymbol{H}}}_{ii}\boldsymbol{x}_i + a_2\hat{\bar{\boldsymbol{H}}}_{ii}\boldsymbol{x}_i^{(3)} + a_3\hat{\bar{\boldsymbol{H}}}_{ii}\boldsymbol{x}_i^{(5)}\right]\right|^2. \tag{35}$$

In this paper, we adopt the trust region reflective algorithm [21] as the regression method.

3.3 Generation of Soft Interference Replica

After computing the nonlinear polynomial coefficients a_1, a_2 and a_3, amplifier output signal $\tilde{\boldsymbol{v}}_i$ can be regenerated by applying the estimated $\bar{G}_i[\cdot]$ to $\boldsymbol{x}_i$. The ACI replica is then generated as follows: At first, the expected values

of the transmit data block are regenerated as a soft modulated signal, using the extrinsic LLR of the channel decoder $\boldsymbol{\gamma}_i$ [18]. If the transmitted signal is modulated by binary phase shift keying (BPSK) and $\boldsymbol{\gamma}_i$ is expressed as $\boldsymbol{\gamma}_i = [\gamma_i(0), \ldots, \gamma_i(k), \ldots, \gamma_i(K-1)]^{\mathrm{T}}$, the soft modulated signal block $\tilde{\boldsymbol{s}}_{\mathrm{d},i} = [\tilde{s}_{\mathrm{d},i}(0), \ldots, \tilde{s}_{\mathrm{d},i}(k), \ldots, \tilde{s}_{\mathrm{d},i}(K-1)]^{\mathrm{T}}$ is given by

$$\tilde{s}_{\mathrm{d},i}(k) = \tanh\left\{\frac{\gamma_i(k)}{2}\right\}. \tag{36}$$

Gray coded quaternary phase shift keying (QPSK) can be expressed as the linear summation of the weighted BPSK symbols. In addition, the quadrature amplitude modulation (QAM) symbols defined in IEEE 802.11ad can be generated by the multiplication and summation of four weighted BPSK symbols. The QPSK symbol $s_{\mathrm{QPSK}}(k)$ and 16 QAM symbol $s_{\mathrm{16QAM}}(k)$ are expressed as

$$s_{\mathrm{QPSK}}(k) = \frac{1}{\sqrt{2}}\{s(k) + js(k+1)\}, \tag{37}$$

$$s_{\mathrm{16QAM}}(k) = \frac{1}{\sqrt{10}}\{2s(k) - s(k)s(k+1)\} + j\frac{1}{\sqrt{10}}\{2s(k+2) - s(k+2)s(k+3)\}, \tag{38}$$

where $s(k)$ represents a BPSK symbol. The soft modulated signals of QPSK and 16 QAM are then generated by substituting $\tilde{\boldsymbol{s}}_{\mathrm{d},i}$ into $s(k)$ in (37) and (38). Furthermore, because the magnitude of soft modulated signals softly limited by the value of the LLR and the LLR tends to be small when a few bits are reliable in the code word. Therefore, the soft replica canceller mitigate the impacts of error propagation.

The soft modulated signal is up-sampled like (3), which is given by

$$\hat{\boldsymbol{x}}_i = \boldsymbol{C}_{\mathrm{TX}}\boldsymbol{O}_2\left[\tilde{\boldsymbol{s}}_{\mathrm{d},i}^{\mathrm{T}}, \mathrm{g}_{\mathrm{d}}^{\mathrm{T}}\right]^{\mathrm{T}}. \tag{39}$$

Then the estimated nonlinear function $\bar{G}_i[\cdot]$ is applied to $\hat{\boldsymbol{x}}_i$, and the ACI soft replica block $\hat{\boldsymbol{q}}_i$ is generated as

$$\hat{\boldsymbol{q}}_i = \boldsymbol{O}_2^{\mathrm{T}}\boldsymbol{\Phi}_{i'i}\hat{\bar{H}}_{i'i}\bar{G}_i[\hat{x}_i]. \tag{40}$$

where the first column vector of $\hat{\bar{\boldsymbol{H}}}_{i'i}$ is $\boldsymbol{O}_2\hat{\boldsymbol{h}}_{i'i}$. Moreover, because we need to estimate $\boldsymbol{h}_{11}, \boldsymbol{h}_{12}, \boldsymbol{h}_{21}$ and $\boldsymbol{h}_{22}$ accurately, we assume that each STA transmits the pilot sequence for both the center frequency, f, and $f + \Delta$.

3.4 Regression Analysis with Data Sequence

In general, the pilot sequence has a smaller PAPR than the data sequence, which incurs an insufficient estimation of nonlinearity in power amplifier for the data sequence.

Figure 4 illustrates a relationship between the output voltage vs. input voltage of the transmit amplifier. The channel model is assumed to be $\bar{\boldsymbol{H}}_{ii} = \boldsymbol{I}$ and $\bar{\boldsymbol{n}}_i = 0$ in (33). The AM-AM curve of the modified Rapp model is depicted in the figure as an exact performance of the amplifier. The

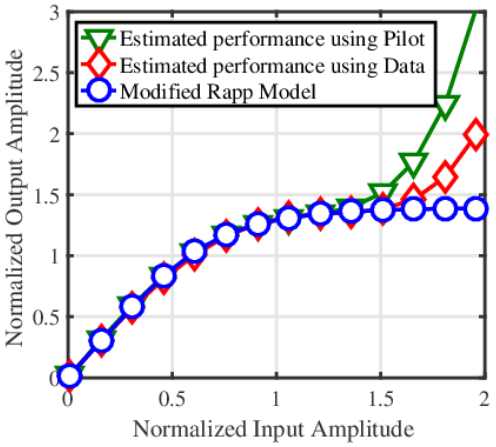

Fig. 4 Performances of output amplitude vs. input amplitude of the transmit amplifier.

other two curves are the estimated performances based on the pilot sequence, and based on the data sequence. In this case, the data sequence is assumed to be perfectly known at the receiver.

The amplitude of the signal before power amplification is normalized by average amplitudes of the pilot and the data sequences. When the roll-off factor for pulse shaping is 0.25, the input amplitude range of the pilot sequence is from 0.8–1.2. On the other hand, the range of the data sequence is from 0.6–1.5 in the case of QPSK.

As can be seen in the figure, these two curves match well with the exact performance, when the input amplitude is lower than 1.2. However, when the input level exceeds 1.2, there is a gap between the performance with the pilot and the exact performance. When the data is used to estimate the nonlinearity, the curve fits well with the exact performance when the input is smaller than 1.5. The mismatch implies that the accuracy of the soft replica $\hat{\boldsymbol{q}}_i$ suffers tremendously from inaccurate nonlinearity estimation on the basis of the pilot.

Therefore, we estimate the nonlinearity from the received data signal $\boldsymbol{y}_i$ and the soft modulated signal $\hat{\boldsymbol{x}}_i$, which is generated from the decoder output LLR $\boldsymbol{\gamma}_i$. Instead of exact $\boldsymbol{x}_i$, $\boldsymbol{x}_i^{(3)}$ and $\boldsymbol{x}_i^{(5)}$, the minimization of (35) is conducted by $\hat{\boldsymbol{x}}_i$. If the reliability of LLR is guaranteed, we can expect accurate results of the regression.

3.5 Complexity of the Cancellation

Applying the proposed ACI cancellation method results in an increase in complexity. At first, the complexity of generating soft ACI replica $\hat{\boldsymbol{q}}_i$ in (40) is dominated by the processing of the nonlinear function $\bar{G}_i[\hat{\boldsymbol{x}}_i]$, and the multiplication of the channel matrix $\hat{\bar{\boldsymbol{H}}}_{i'i}$. Furthermore, $\hat{\boldsymbol{x}}_i^{(5)}$ in $\bar{G}_i[\hat{\boldsymbol{x}}_i]$ needs $4 \times 2K$ multiplications, and the multiplication of $\hat{\bar{\boldsymbol{H}}}_{i'i}\bar{G}_i[\hat{\boldsymbol{x}}_i]$ needs $2K \times 2K$ multiplications. In addition, the regression method for nonlinearity estimation and repetition of decoding also increases computational complexity. Moreover, al-

though complexity reduction is not mentioned in this paper, it is necessary to exploit some complexity reduction method if the complexity of ACI cancellation is not acceptable.

4. Performance Evaluations

In this section, we discuss the performance of the proposed iterative multichannel receiver with the ACI canceller, using link level and system level computer simulations.

4.1 Link Level Simulation

At first, in order to investigate the validity of the proposed ACI cancellation scheme, link level simulations were conducted. The simulation parameters are summarized in Table 1. The DFT window size K is 512 points. One data frame is composed of 1500 B. The channel model is 60 GHz living room channel model specified in [22], which applies beamforming in line of sight (LOS) environments. We use the same parameters of the modified Rapp model in Sect. 2, where the OBO is 0.6 dB. We evaluated the performances for the two following scenarios.

In scenario 1, transmit signals of both STA1 and STA2 obey QPSK signaling that is encoded by half-rate LDPC codes, specified in IEEE802.11ad. Here, we focus on severe ACI environments where STA2 is located very close to the AP, when compared with STA1. The average difference of the received power P_{diff} is defined when ACI is neglected ($q_1(k) = q_2(k) = 0$), which is given by

$$P_{\text{diff}} = 10 \log_{10} \frac{\mathbb{E}\left\{|r_2(k)|^2\right\}}{\mathbb{E}\left\{|r_1(k)|^2\right\}}. \tag{41}$$

Figure 5 illustrates the spectral mask of IEEE 802.11ad and the 16 QAM signal spectra with an OBO of 0.6 dB. In this figure, the leaked spectrum power is approximately −(25–20) dBr, compared with the main spectrum. Moreover, this spectrum leakage is allowed by the regulation of the spectral mask. Thus, the power of ACI on the CH1 signal become P_{diff} = 20–25 dB. In the following simulations, the averaged received power from STA2 is assumed to be higher than 20 dB or 25 dB, when compared with that of STA1.

Figures 6 and 7 show the BER performances of transmitted data from STA1, where P_{diff} = 20 dB and 25 dB. In each figure, the following curves are depicted: the ideal case without ACI (w/o ACI), the worst case under ACI without any interference canceller (w/ ACI, w/o canceller), the proposal under ACI with interference canceller of pilot based nonlinearity estimation (w/ ACI, w/ canceller (P1) and (P2)), and another proposal under ACI with the interference canceller of data based nonlinearity estimation (w/ ACI, w/ canceller

Table 1 Link level simulation parameters.

Modulation and coding rate in **scenario 1**	STA1: QPSK, rate 1/2 STA2: QPSK, rate 1/2
Modulation and coding rate in **scenario 2**	STA1: QPSK, rate 13/16 STA2: 16QAM, rate 3/4
DFT window size	512
time synchronization	perfect
Frame length	1500 byte
Channel model	60 GHz living room channel model [22]
Number of iteration for cancellation	1, 2

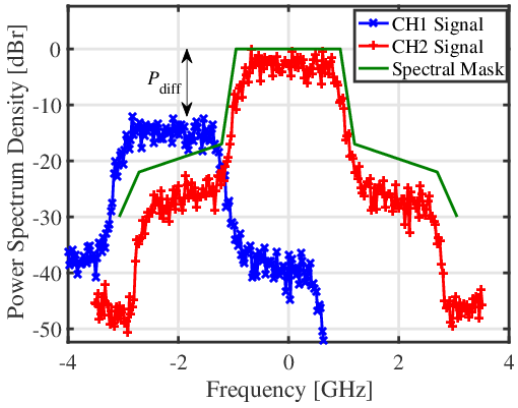

Fig. 5 Signal spectra and spectral mask.

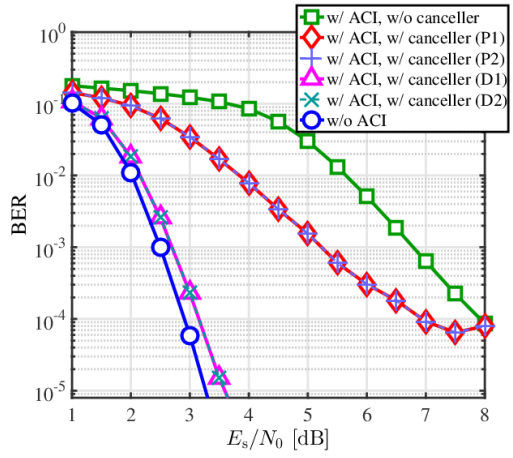

Fig. 6 BER performance in scenario 1 (P_{diff} = 20 dB).

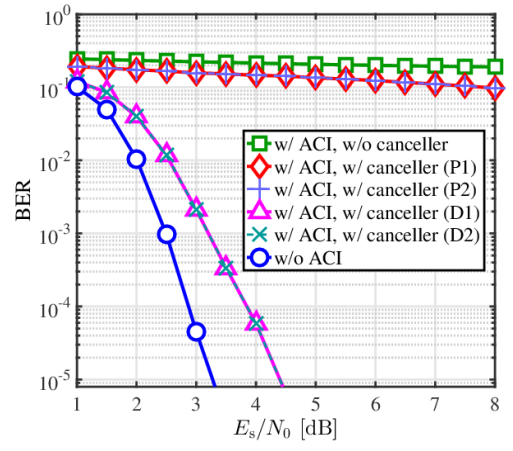

Fig. 7 BER performance in scenario 1 (P_{diff} = 25 dB).

(D1) and (D2)), where the index 1, and 2 behind P and D indicate the number of iteration for cancellation. In both Figs. 6 and 7, the STA2 signal is detected almost completely, and the soft modulated signal $\tilde{\boldsymbol{s}}_{\mathrm{d},2}$ is equal to the transmitted signal $\boldsymbol{s}_{\mathrm{d},2}$. Therefore, increasing the iteration number is ineffective here, because the soft ACI replica $\hat{\boldsymbol{q}}_2$ is not changed by the iteration number and $\hat{\boldsymbol{q}}_1$ is negligibly small.

In Fig. 6, when the ACI from STA2 exists and ACI cancellation is not applied, BER = 10^{-5} is not achievable, even with E_{s}/N_0 = 8 dB. Moreover, as mentioned in Sect. 3.4, even if we apply ACI cancellation with pilot based nonlinearity estimation, BER = 10^{-5} is not attained because of the insufficient accuracy of the regression for non-linear parameters. On the other hand, when ACI cancellation is carried out while using the data sequence, the required E_{s}/N_0 for achieving BER = 10^{-5} is only 0.3 dB higher than the ideal case.

Furthermore, because the ACI from STA2 is more severe in Fig. 7, ACI cancellation with pilot based nonlinearity estimation is no longer effective. Even in this case, the degradation is only 1 dB at BER = 10^{-5}, with the aid of data based nonlinearity estimation.

In scenario 2, STA1 and STA2 transmit QPSK signals with a coding rate of 13/16, and 16QAM signals with a coding rate of 3/4. In this scenario, the PAPR of STA2 signal is high, and more spectrum leakage occurs. Figure 8 characterizes the BER performances when P_{diff} = 20 dB. As shown in Fig. 8, the BER performance of the proposed scheme is limited, when compared with that of Fig. 6. In the proposed scheme, nonlinearity is estimated using twofold up-sampled received signals. However, two-fold up-sampling is insufficient for estimating ACI perfectly. Moreover, the channel estimation error also affects soft replica generation. In the 16QAM signaling with the higher PAPR when compared to QPSK signaling, residual interference induced by the imperfection of the nonlinear estimation becomes severe. As a result, the BER performance of the proposed method in Fig. 8 is worse than that in Fig. 6.

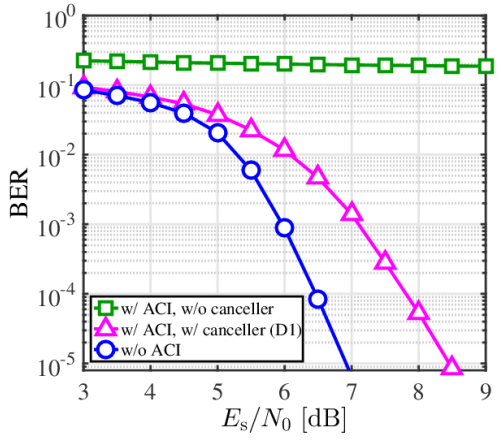

Fig. 8 BER performance in scenario 2 (P_{diff} = 20 dB).

4.2 System Level Simulations

In this subsection, we discuss system level characteristics of multi-channel communication systems with the proposed ACI cancellation scheme, in an uplink transmission scenario. Figure 9 illustrates a system model of multichannel utilization in mmW communication systems. In this system, AP has three directional sectors [23], and we assume that multiple channels are used in the single sector. The number of available channels is four: CH1 (f_1 = 58.32 GHz), CH2 (f_2 = 60.48 GHz), CH3 (f_3 = 62.64 GHz), and CH4 (f_4 = 64.80 GHz), where f_i denotes the center frequency of the i-th channel. Moreover, in this simulation, plural stations in the same sector transmit data sequences via different channels.

Figure 10 illustrates a flow of resource management for multichannel allocations. The first STA that generate packet is set as "primary STA". When the other STAs request packet transmissions, they are set to "secondary STA". Unused channels are assigned to the secondary STAs. Moreover, plural STAs simultaneously transmit signals via multichannels. In the simultaneous transmissions, received antenna directivity is directed to the primary STA, and secondary STAs can transmit signals if the received power satisfies the minimum required received signal to noise power ratio (SNR). This is because the analog beam-former in each sector can steer one direction over all the channels. Each STA selects a modulation and coding rate from Table 2.

To mitigate the impacts of interference as much as possible, the channel allocation order is set to CH1, CH3, CH2, and CH4. Thus, interference occurs when more than three

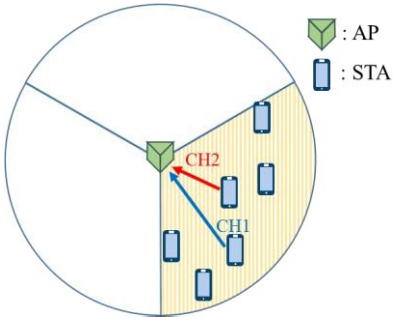

Fig. 9 System model of multichannel utilizations in single sector.

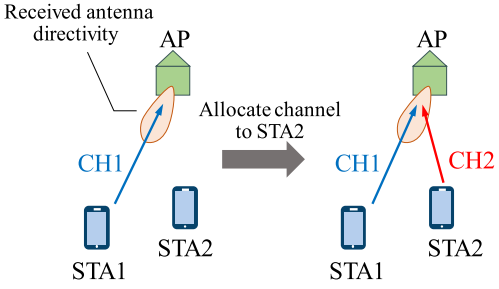

Fig. 10 Flow of resource management for multichannel allocations.

Table 2 Required SNR for FER = 10^{-3}.

Modulation and coding rate	Required SNR [dB]
BPSK, rate 1/2	0.5
BPSK, rate 5/8	2.0
BPSK, rate 3/4	2.4
QPSK, rate 1/2	3.0
QPSK, rate 5/8	4.5
QPSK, rate 3/4	5.8
QPSK, rate 13/16	7.0
16QAM, rate 1/2	10.1
16QAM, rate 5/8	13.5
16QAM, rate 3/4	16.0

Table 3 Parameters of single sector simulations.

Number of STAs	10
Transmission power	10 dBm
Noise power	-173.82 dBm/Hz
Noise figure	10 dB
Path loss	Obeying channel model [22]
Traffic generation model	Traffics are generated by Poisson process. Average arrival rate is 2 or 4
Maximum distance between AP to STA	15 m
Traffic size	200 MB
Maximum data size in one frame	8000 B
Observation period	10 s

STAs transmit signals at the same time. An adjacent channel is allocated if P_{diff} between the previously assigned channel and its adjacent channels is lower than 10 dB. This is because ACI can be ignored with the assistance of forward error correction. In other words, if P_{diff} is higher than 10 dB, the adjacent channel is not allocated in this system. Therefore, the number of available channels decreases when an unacceptable ACI occurs.

In the case with the ACI canceller, even if P_{diff} is higher than 10 dB, it is possible that adjacent channels are available, owing to the functionality of the interference cancellation. However, a residual interference cannot be ignored when P_{diff} is higher than 30 dB. As a result, the adjacent channel is unavailable. Thus, we apply a criterion that the adjacent channel is activated if $10\,\text{dB} \leq P_{\text{diff}} \leq 30\,\text{dB}$, otherwise it is not activated. In addition, as mentioned in the previous section, the required received SNR is slightly increased due to the residual interference. Therefore, we add a 2 dB margin to the required received SNR in Table 2 when we apply the ACI cancellation.

Table 3 specifies the simulation parameters. Ten STAs are randomly distributed within the area in each observation period. We calculated the system throughput performance, which is defined as the total throughput of all the transmitted packets.

Figure 11 shows the complementary cumulative distribution function (CCDF) of the system throughput. Moreover, (2) and (4) indicate cases where the average arrival rates of the Poisson process are 2 and 4, respectively. When the average arrival rate is 2, the simultaneous transmission

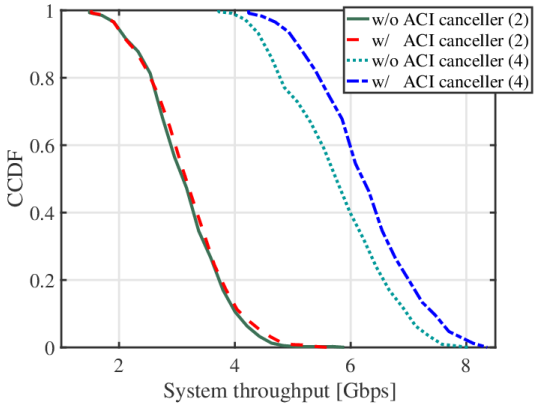

Fig. 11 CCDF of system throughput.

of more than three STAs rarely occurs. Therefore, the maximum throughput is lower than 6 Gbps. In this case, the proposed ACI canceller is not so effective in improving the throughput, because the system does not severely suffer from ACI. On the other hand, when the average arrival rate is 4, a 20% improvement can be observed at 6 Gbps in the figure. Without the functionality of ACI cancellation, the number of available channels tends to decrease if many STAs request transmission at the same time. In this situation, the proposed scheme is a promising technique for the improvement of throughput performance.

5. Conclusion

This paper proposed an iterative cancellation scheme for ACI in mmW systems, with the assistance of a nonlinear estimator for the power amplifier. The major contribution of this paper was to reveal how to generate the soft interference replica, and the primary problem to be solved was how to improve the accuracy of nonlinearity estimation. In order to achieve sufficient quality of the nonlinearity estimation, regression analysis using the data sequence was proposed.

Link level computer simulations confirmed that the proposed scheme can effectively suppress ACI to an acceptable level. Additionally, we also confirmed that the proposed ACI canceller can improve system level throughput performance in multichannel access systems.

References

[1] Q.C. Li, N. Huaning, A.T. Papathanassiou, and W. Geng, "5G network capacity: Key elements and technologies," IEEE Veh. Technol. Mag., vol.9, no.1, pp.71–78, March 2014.
[2] E. Larsson, O. Edfors, F. Tufvesson, and T. Marzetta, "Massive MIMO for next generation wireless systems," IEEE Commun. Mag., vol.52, no.2, pp.186–195, Feb. 2014.
[3] T.S. Rappaport, S. Sun, R. Mayzus, H. Zhao, Y. Azar, K. Wang, G.N. Wong, J.K. Schulz, M. Samimi, and F. Gutierrez, "Millimeter wave mobile communications for 5G cellular: It will work!," IEEE Access, vol.1, no.1, pp.335–349, May 2013.
[4] J.G. Andrews, "Seven ways that HetNets are a cellular paradigm shift," IEEE Commun. Mag., vol.51, no.3, pp.136–144, March 2013.
[5] B. Razavi, "Design of millimeter wave CMOS radios: A tutorial,"

IEEE Trans. Circuits Syst. I, vol.56, no.1, pp.4–16, Jan. 2009.
[6] S. Emami, C.H. Doan, A.M. Niknejad, and R.W. Broderson, "A highly-integrated 60-GHz CMOS front-end receiver," ISSCC Dig. Tech. Papers, pp.190–191, Feb. 2007.
[7] N. Saito, T. Tsukizawa, N. Shirakata, T. Morita, K. Tanaka, J. Sato, Y. Morishita, M. Kanemaru, R. Kitamura, T. Shima, T. Nakatani, K. Miyanaga, T. Urushihara, H. Yoshikawa, T. Sakamoto, H. Motozuka, Y. Shirakawa, N. Yosoku, A. Yamamoto, R. Shiozaki, and K. Takinami, "A fully integrated 60-GHz CMOS transceiver chipset based on WiGig/IEEE 802.11ad with built-in self calibration for mobile usage," IEEE J. Solid-State Circuits, vol.48, no.12, pp.3146–3159, Dec. 2013.
[8] IEEE Std. 802.11ad, "Part 11: Wireless LAN Medium Access Control (MAC) and Physical Layer (PHY) Specifications, Amendment 3: Enhancements for Very High Throughput in the 60 GHz Band," Dec. 2012.
[9] W. Gerhard and R. Knoechel, "Improvement of power amplifier efficiency by reactive chireix combining, power back-off and differential phase adjustment," Proc. IEEE MTT -IMS, pp.1887–1890, San Francisco, USA, June 2006.
[10] S.P. Stapletonancl and F.C. Costescu, "An adaptive predistorter for a power amplifier based on adjacent channel emissions," IEEE Trans. Veh. Technol., vol.41, no.1, pp.49–56, Feb. 1992.
[11] M. Rawat, K. Rawat, and F.M. Ghannouchi, "Adaptive digital predistortion of wireless power amplifiers/transmitters using dynamic real-valued focused time-delay line neural networks," IEEE Trans. Microw. Theory Techn., vol.58, no.1, pp.95–104, Jan. 2010.
[12] K. Cavers, "Amplifier linearization using a digital predistorter with fast adaptation and low memory requirements," IEEE Trans. Veh. Technol., vol.39, no.4, pp.374–382, Nov. 1990.
[13] X. Wang and H.V. Poor, "Iterative (turbo) soft interference cancellation and decoding for coded CDMA," IEEE Trans. Commun., vol.47, no.7, pp.1046–1061, July 1999.
[14] S. Tomasin, A. Gorokhov, H. Yang, and J. Linnartz, "Iterative interference cancellation and channel estimation for mobile OFDM," IEEE Trans. Wireless Commun., vol.4, no.1, pp.238–245, Jan. 2005.
[15] R.G. Gallager, "Low density parity check codes." IRE Trans. Inform. Theory, vol.IT-8, no.1, pp.21–28. Jan. 1962.
[16] T. Richardson, M. Shokrollahi, and R. Urbanke, "Design of capacity-approaching irregular low density parity check codes," IEEE Trans. Inform. Theory, vol.47, no.2, pp.619–637, Feb. 2001.
[17] M.J.E. Golay, "Multislit spectroscopy," J. Opt. Soc. Am., vol.39, no.6, pp.437–444, June 1949.
[18] L. Hanzo, T. Liew, and B. Yeap, Turbo Coding, Turbo Equalisation and Space-Time Coding, Wiley, 2002.
[19] V. Erceg, M. Messe, A. Tarighat, M. Boers, J. Trachewsky, and C. Choi, "60 GHz impairments modeling," IEEE Doc 802.11-09/1213r1, Nov. 2009.
[20] S. Banedetto and E. Biglieri, Principle of Digital Transmission with Wireless Applications, Kluwer Academic/Plenum Publishers, New York, 1999.
[21] T.F. Coleman and Y. Li, "An interior, trust region approach for nonlinear minimization subject to bounds," SIAM J. Optim., vol.6, no.2, pp.418–445, May 1996.
[22] A. Maltsev, et al., "Channel models for 60 GHz WLAN systems," IEEE Doc. 802.11-09/0334r8, May 2010.
[23] K. Sakaguchi, E.M. Mohamed, H. Kusano, M. Mizukami, S. Miyamoto, R.E. Rezagah, K. Takinami, K. Takahashi, N. Shirakata, H. Peng, T. Yamamoto, and S. Nanba, "Millimeter-wave wireless LAN and its extension toward 5G heterogeneous networks," IEICE Trans. Commun., vol.E98-B, no.10, pp.1932–1948, Oct. 2015.

Noboru Osawa received B.E. and M.E. degrees in communications engineering from Osaka University, Osaka, Japan, in 2014 and 2016, respectively. He is currently a Ph.D. student at the Graduate school of Engineering, Osaka University.

Shinsuke Ibi received a B.E. degree in Advanced Engineering from Suzuka College of Technology, Japan, in 2002, and M.E. and Ph.D. degrees in communication engineering from Osaka University, Japan, in 2004 and 2006, respectively. From 2005–2006, he was a visiting researcher at the Centre for Wireless Communications at The University of Oulu, Finland. In 2006, he joined the Graduate School of Engineering, Osaka University, and he is currently an Associate Professor in the department of Information and Communications Technology at Osaka University. From 2010–2011, he was a visiting researcher at The University of Southampton in the UK. His research interests include EXIT-based coding theory, iterative detection, digital signal processing, cognitive radio, and communication theory. He received the 64-th and 71-st Best Paper Awards from the IEICE, and the 24th Telecom System Technology Award from the Telecommunication Advancement Foundation. He is a member of the IEEE.

Seiichi Sampei received B.E., M.E. and Ph.D. degrees in electrical engineering from Tokyo Institute of Technology, Japan, in 1980, 1982 and 1991, respectively. From 1982–1993, he was with the Communications Research Laboratory, Ministry of Posts and Telecommunications. Moreover, from 1991–1992, he was at The University of California, Davis, as a visiting researcher. In 1993, he joined the Faculty of Engineering, Osaka University, and he is currently a Professor in the department of Information and Communications Technology, Osaka University. He has developed adaptive modulation, intelligent radio transmission/access, cognitive wireless networking, and wireless distributed network techniques. He received the Shinohara Young Engineering Award, the Achievements Award, Communications Society Best Paper Award and Best Paper Award from the IEICE, the Telecom System Technology Award from the Telecommunication Advancement Foundation, the DoCoMo Mobile Science Award from the Mobile Communication Fund, and the Ericsson Telecommunications Award. He is a member of the Institute of Image Information and Television Engineers (ITE) and a Fellow of the IEEE.